The Design and Analysis of Piezoresistive Shuriken-Structured Diaphragm Micro-Pressure Sensors

Taotao Guan, Fang Yang, Wei Wang, Xian Huang, Boyan Jiang, and Dacheng Zhang

***Abstract*— This paper presented a novel 0–3 kPa piezoresistive pressure sensor with high sensitivity and linearity. A shuriken-structured diaphragm (SSD) is designed for the first time to solve the conflict between the sensitivity and linearity for piezoresistive pressure sensors. A trade-off between the stress on the diaphragm edge and the deflection of the diaphragm was achieved by this SSD design according to the numerical simulation. The effects of the glass substrate and the passivation films on the sensing performance were also studied numerically and experimentally. The experimental results indicated the present pressure sensor had a sensitivity of 4.72 mV/kPa/V and a linearity of 0.18 %FSO (full scale output) in the pressure range of 0–3 kPa, which were 28.3% and 50% better than the previous works. [2016-0101]**

***Index Terms*— High sensitivity and linearity, piezoresistive pressure sensor, shuriken-structured diaphragm.**

I. Introduction

INTRAOCULAR pressure (IOP) and intracranial pressure (ICP) measurements are of great significance for health-care. High IOP may cause glaucoma [2]. High ICP in traumatic brain injury may lead to higher mortality [3]. Traditional IOP and ICP measurements usually require anesthesia and lumbar puncture, which lack precision and incompetent for long-term monitoring. Implantable real-time IOP and ICP monitors with high precision and sensitivity are highly in demand. The IOP and ICP of healthy adults usually range 1.47-2.79 kPa and 0.78-1.76 kPa, respectively. Similar to blood pressure measurements [4], 0.1 mm Hg in a 20mm Hg full pressure range is demanded. This means that the nonlinearity error of pressure sensors has to be smaller than 0.5% FSO. Therefore, a pressure sensor with a high sensitivity and linearity in 0-3 kPa is required for according IOP and ICP monitoring applications. This type sensor also can be widely used in automobiles [5], smart homes [6] and process control [7].

Unfortunately, it is a challenge to get a piezoresistive diaphragm-shaped pressure sensor with a high sensitivity and linearity at the same time [4]. Lin et al. [8] studied the sensitivity and linearity of piezoresistive pressure sensors and indicated that a thin sensing diaphragm was helpful to increase the device sensitivity but also caused a higher nonlinearity error and hysteresis. Chiou et al. [9] investigated the pressure nonlinearity of devices with thin diaphragms under high residual stresses, which showed the sensitivity and linearity of piezoresistive pressure sensors were closely related to the residual stresses of passivation films. In the research of Matsuda *et al.* [10], nonlinear piezoresistance effects in silicon were carefully studied and the results indicated that for <110> piezoresistors, the longitudinal and transverse piezoresistive coefficients were different and the piezoresistance effect had coefficients of the second-order and third-order, which will lead to a poor linearity for piezoresistive pressure sensors.

Several diaphragm structures have been designed to address the above conflicts between the sensitivity and linearity of piezoresistive pressure sensors. A peninsula-structured diaphragm [11] was designed to decrease the nonlinearity. Beam-membrane [12] and square-diaphragm with a rectangular central boss [13] were used to suppress the nonlinearity. However, the above designs gained a better nonlinearity at the expense of decreasing sensitivity. The square-diaphragm with a rectangular central boss [13] also achieved high overload range. However, due to the adverse effect of acceleration, the square-diaphragm device also had a stability issue. In this work, a shuriken-structured diaphragm (SSD) is proposed for the first time to improve both sensitivity and linearity for the piezoresistive pressure sensor by carefully trading off the stress on the beam edge and the deflection of the sensing diaphragm.

Section II mainly discussed the numerical simulations of the SSD design. The whole fabrication process was presented in Section III. Section IV showed the experimental results. Conclusion was given in section V.

II. Design of the SSD Sensor

The SSD sensor structure was introduced in detail. In order to improve both sensitivity and linearity, systematic FEM (finite element method) analysis was made to optimize the stress distribution within the piezoresistive area. The SSD showed unique advantages over previous designs. The stresses caused by the packaging and the passivation were also analyzed in details.

Manuscript received May 11, 2016; revised August 8, 2016 and October 22, 2016; accepted November 11, 2016. This work was supported by the National Science and Technology Major Project of China under Grant 2011ZX02507-001-002. Subject Editor Y. Zohar. *(Corresponding author: Dacheng Zhang.)*

The authors are with the Institute of Microelectronics, Peking University, Beijing 100871, China (e-mail: happy_gtt@163.com; yangfang@pku.edu.cn; wangw@ime.pku.edu.cn; huangxian2010@pku.edu.cn; jiangby@ime.pku.edu.cn; dchzhang@ime.pku.edu.cn).

Color versions of one or more of the figures in this paper are available online at http://ieeexplore.ieee.org.

Digital Object Identifier 10.1109/JMEMS.2016.2628781

A. Sensitivity and Nonlinearity of Piezoresistive Pressure Sensor

According to the classical piezoresistance theory [14], the sensitivity and nonlinearity of a piezoresistive pressure sensor based on the full Wheatstone bridge circuit [15] can be derived as,

$$SENS = \frac{\overline{Sx\_y\_l} + \overline{Sx\_y\_t}}{2} \times \frac{\pi 44}{2} \times Vs/P \tag{1}$$

$$NONL = \frac{\left(\overline{Sx\_y\_l}\right)^2 - \left(\overline{Sx\_y\_t}\right)^2}{4} \times \left(\frac{\pi 44}{2}\right)^2 \times Vs/Vfso \tag{2}$$

where *SENS* and *NONL* are the sensitivity and nonlinearity error of piezoresistive pressure sensors, *Sx_y* is the difference between stress in the x direction and stress in the y direction in the piezoresistive area, l and t represent longitudinal and transverse piezoresistors, $\pi_{44}/2$ is the <1 1 0> direction piezoresistive coefficient ($69 \times 10^{-11}\mathrm{Pa}^{-1}$ [9]), *Vs* is the supply voltage, P is pressure, and V_{fso} is the full scale voltage output.

Based on the membrane theory [16], for typical square diaphragm-shaped pressure sensors, as in Equation 3, a large L/H is required for tiny pressure measurements to guarantee enough stress (i.e., the output voltage) for high sensitivity.

$$\sigma_{sd} = 0.308P\left(\frac{L}{H}\right)^2 \tag{3}$$

Where σ_{sd} is the maximum stress (nearly *Sx_y* in the piezoresistive area), L is the diaphragm length, H is diaphragm thickness.

Due to the high L/H, the large-deflection effect [16] will be induced, which will induce the pressure nonlinearity. Therefore, unwanted nonlinearity error was caused. By increasing the local stiffness of a diaphragm, the non-linear large-deflection effect can be suppressed to a considerable extend. It should be remembered that flexural stiffness [17] is:

$$D = \frac{EH^3}{12\left(1\text{-}\mu^2\right)} \tag{4}$$

Where E is Young‘s modulus, μ is Poisson‘s ratio.

Previous tiny pressure sensors were all based on the above strategy [11]–[13]. Applying this design thought, the proposed SSD sensor was made and showed high sensitivity and linearity. It should be noticed that there is still room for further improvement in the sensor performance.

B. The Principle of the SSD

In this work, a shuriken-structured diaphragm (SSD), as shown in Figure 1, is proposed for the first time. A cross beam with the shuriken design (Figure 1a) not only suppressed the large deflection, i.e. decreased the nonlinearity, but also increased the stress on the diaphragm edge, the key parameter for sensitivity improvement. The shuriken-structured beam was the key component of the present SSD design. Based on Equation 4, as shown in Figure 1c, on the membrane edge, the beam width was designed as small as possible to decrease the local flexural stiffness and guaranteed a not bad sensor sensitivity, while at the membrane center, the beam width was large enough to increase the local flexural stiffness for a better sensing linearity.

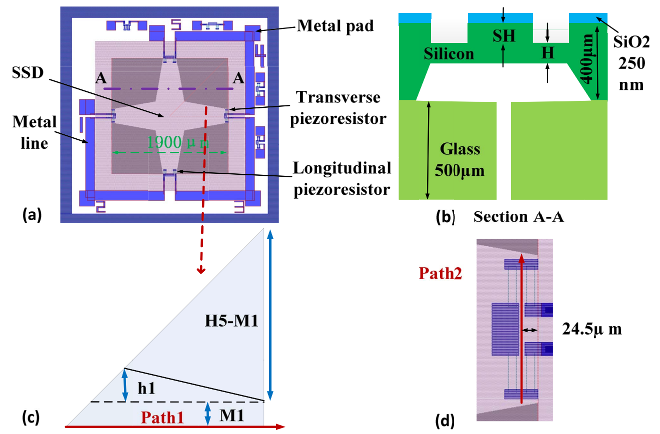

Fig. 1. (a) Proposed SSD sensor structure (b) Section A-A (c) 1/8 SSD plan view and Path1 definition (d) Path2 definition.

The size of the SSD sensor was 3.4×3.4 mm^2. The diaphragm length was 1900 μm (Figure 1a) and covered by 250 nm SiO_2 as the passivation film (Figure 1b). A hole with diameter of 1 mm was drilled through the glass substrate for differential pressure measurement (Figure 1b). Piezoresistors were connected by aluminum wires and formed a full Wheatstone bridge (Figure 1a). The pressure were thereby converted to the electrical readout through the Wheatstone bridge circuit. The details of the configuration of piezoresistors were shown in Design IV in [11].

Given diaphragm length L, there were four parameters to be designed: membrane thickness H and shuriken thickness *SH* shown in Figure 1b; beam width *M1* on the diaphragm edge and the critical parameter *Ratio* representing the slope of the linear gradient beam shown in Figure 1c.

$$Ratio = \frac{h1}{(H5 - M1)} \tag{5}$$

Two paths, as shown in Figure 1c and 1d, were adopted to monitor the stress distribution during the pressure sensor design. Path1 went from the diaphragm center to the diaphragm edge. Path2 was the midline of the transverse piezoresistors and paralleled to the diaphragm edge.

C. Geometry Design of the SSD

Based on Equation 3, the initial silicon membrane thickness H was designed to 19 μm. On the one hand, the membrane can be fabricated by KOH etching with high yield. On the other hand, the membrane can be further structured by shuriken to get proper stress distribution.

FEM simulation results for 19 μm diaphragm pressure sensor were shown in Figure 2. The maximal Sx_y was only about 6 MPa (Figure 2a). When distance from beam center increased, the stress Sx_y decreased from 5.86 to 5.72 MPa, which is about 2.4% of 5.86 MPa (Figure 2b).

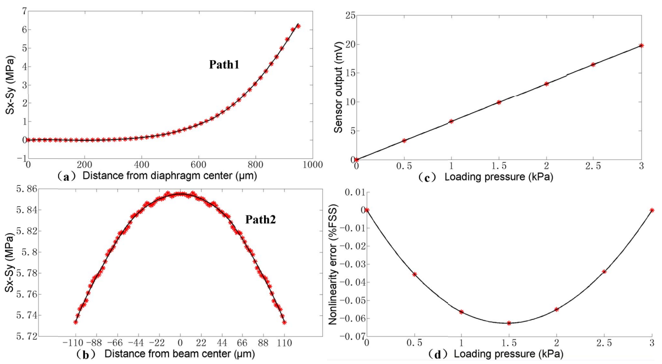

Fig. 2. FEM simulation results for square diaphragm (H = 19 μm, L = 1900 μm): the stress distribution (a) from diaphragm center to edge and (b) from beam center to beam edge; (c) Sensor output and (d) Nonlinearity error versus loading pressure.

From Figure 2d, it can be seen that though sensor linearity was good (0.07 %FSO), the sensitivity was terrible. It can be seen more directly from Figure 2c that the sensitivity was about 1.33 mV/kPa/V, which was too small to be used. Based on nonlinear theory of large deflection and the stress distribution shown in Figure 2b, the nonlinearity was caused mainly by piezoresistive regional stress asymmetry, but not membrane large deflection.

Based on piezoresistance effect (Equation 1), the corresponding stress Sx_y should be approximately 20 MPa to get 70 mV FSO under 3 kPa air pressure and 5V DC supply. It can be obtained from ANSYS simulation. High stress Sx_y lied nearly on the diaphragm edge where piezoresistors should be placed. Limited by the piezoresistors configuration in [11], beam width $M1$ on the diaphragm edge was designed to 220 μm. $H5$ and *Ratio* were determined by Equation 5 and 6. Given L =1900 μm, *SH* and *Ratio* were the only two variables in Figure 1.

$$H5 = \frac{L}{2} = 950\ \mu\text{m} \tag{6}$$

There were only SH and Ratio to be designed. And SH needed to be designed firstly. To get proper shuriken thickness SH, we assumed that *Ratio* (Equation 6) = 0. The sensitivity and linearity simulation results with shuriken thickness varying from 2 to 18 μm were shown in Figure 3. It can be seen that if the shuriken thickness increased, the sensitivity and nonlinearity error increased at the same time. Shuriken thickness was finally designed to 16 μm to get nearly 70 mV full scale output. But the nonlinearity error was about 0.7 %FSO and still not that satisfying.

Ratio was one of the most important parameters for the SSD structure. The performance optimization of the sensor with ratio ranging from 1/20-10/20 was displayed in Figure 4. Figure 4a showed that when the ratio increased, Sx_y on the beam edge decreased gradually. On the beam edge, stress Sx_y increased abruptly where piezoresistors should not be put as it was adverse for the device linearity. The stress path in Figure 4b was located in the bisector of the transverse piezoresistors, parallel to the edge of the SSD. Far away from the beam center (about 100μm) shown in Figure 4b,

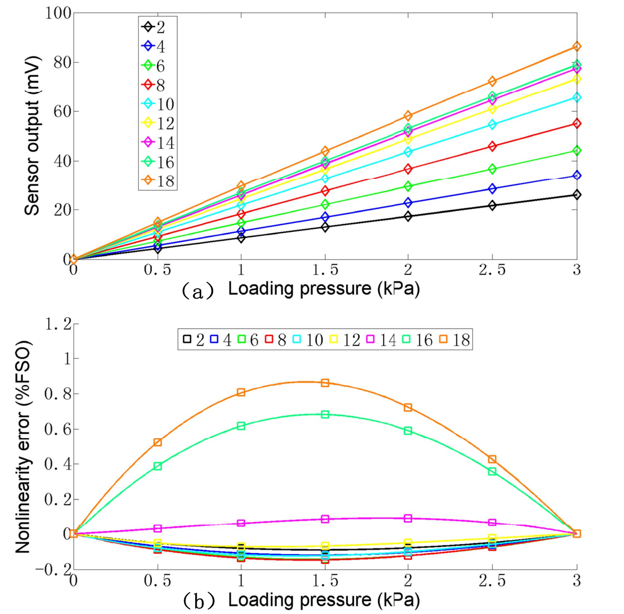

Fig. 3. FEM simulation results for shuriken thickness with SH ranging from 2-18 μm (Ratio=0, L=1900 μm): (a) Sensor output and (b) Nonlinearity error versus loading pressure.

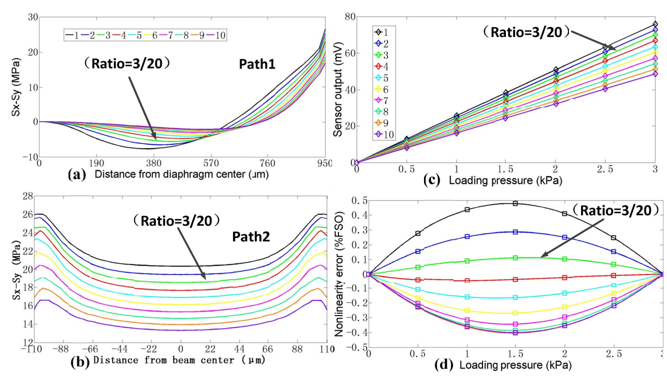

Fig. 4. Performance optimization with Ratio ranging from 1/20-10/20: The stress Sx_y distribution (a) from diaphragm center to edge and (b) from beam center to beam edge; (c) Sensor output and (d) Nonlinearity error versus loading pressure.

stress Sx_y reduced soon, where piezoresistors should not be placed, because it was both harmful to the device linearity and sensitivity. Furthermore, Figure 4b revealed that the overall stress was lowered and stress distribution was altered with the increase of *Ratio*. By trading off the sensitivity (Figure 4c) and linearity (Figure 4d) of the sensor, the ratio was finally determined to 3/20. The simulation indicated that the SSD sensor had a high sensitivity of 4.67 mV/kPa/V and a low nonlinearity of less than 0.1 %FSO. The optimization of Ratio decreased the nonlinearity from 0.7 %FSO to only 0.1 %FSO.

The thin area of the SSD was 3 μm thick. FEM simulation results for 3 μm diaphragm pressure sensor were shown in Figure 5. When distance from diaphragm center increased, the stress Sx_y increased, especially more rapidly from 800 μm (Figure 5a). When distance from beam center increased, the stress Sx_y floated up and down, but was still within 70-71.5 MPa range, which was about 2.1% of 71.5 MPa

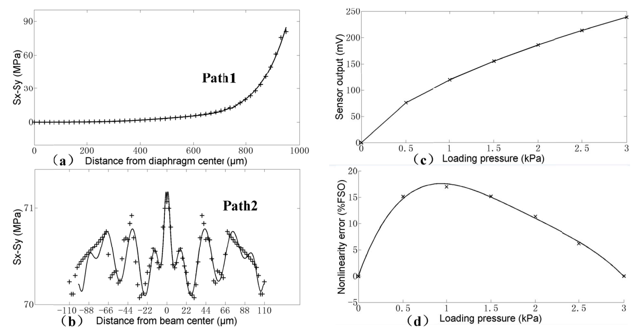

Fig. 5. FEM simulation results for square diaphragm (H = 3 μm, L = 1900 μm): the stress distribution (a) from diaphragm center to edge and (b) from beam center to beam edge; (c) Sensor output and (d) Nonlinearity error versus loading pressure.

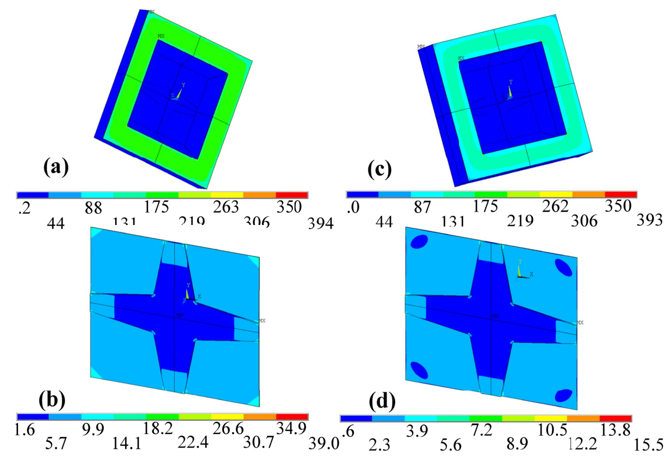

Fig. 6. Von Mises stress (MPa) distribution for the whole sensor without (a) and with (c) bonded glass (thickness = 500 μm); Von Mises stress distribution for the sensing membrane without (b) and with (d) bonded glass.

(Figure 5b). From Figure 5c, it can be seen that though sensor sensitivity was very high (about 16.7 mV/kPa/V), the linearity was very terrible. It can be seen more directly from Figure 5d that nonlinearity error was about 18 %FSO, which was unacceptable for sensor application. Based on nonlinear theory of large deflection and the approximately uniform stress distribution shown in Figure 5b, the bad linearity was caused mainly by large deformation, but not piezoresistive regional stress asymmetry.

In general, for 3 μm thickness films, though the sensitivity was satisfactory (16.7 mV/kPa/V), the nonlinearity error was bad (18 %FSO). For 19 μm thickness films, though the nonlinearity error was pleasing (0.07 %FSO), the sensitivity was poor (1.33 mV/kPa/V). As for the proposed SSD sensor, the sensitivity was 4.67 mV/kPa/V and the nonlinearity error was less than 0.1 %FSO. High sensitivity and linearity were achieved simultaneously.

D. FEM Analysis for Stress Cushioning-Effect of the Bonded Glass

Pressure sensor chips can be used only after being adhered to various baseboards by packaging glue. The glue solidification can help get enough bonding strength between sensor chips and baseboards. However, the glue solidification also changed the glue volume and thus caused contact stress. The packaging stress can be spread to the sensing membrane and made it deformed. The time and temperature instability of glue can affect the sensor performance. As for static characteristics, the stress deformed the sensing membrane without loading pressure and thus increased the sensor zero-point output voltage.

No matter how many factors influenced the chip, the packaging stress needed to be spread to the sensing membrane by chip body. Therefore, the packaging stress spreading characteristics of the sensor chip was important. It can be easily known that the weak stress spreading ability was wanted for better sensor performance.

Sensor stress spreading ability for SSD sensors with bonded glass was weaker than these without glass. And the sensor performance for SSD sensors with glass was better. For the glue solidification process, at the beginning the glue was put between the sensor chips and baseboards and the stress was supposed to be zero, then the glue was cured and its volume was changed, finally stress was induced between the sensor bottom and glue. About the thermal mismatch phenomenon, at the beginning the thin membrane was deposited by LPCVD at high temperature and the stress was zero, then temperature decreased to room temperature and the membrane volume was changed due to thermal mismatch, finally stress was caused. The packaging stress and thermal mismatch stress were both biaxial plane stress. To a certain extent, it was rational to use thermal mismatch stress to simulate packaging stress.

Figure 6 showed the stress cushioning-effect of the glass. In Figure 6a and 6c, the same thing was that stress was high at a location with sudden changes of geometry and stress distribution was similar. Given the same packaging stress, the membrane stress with bonded glass (Figure 6d) was much less than these without glass (Figure 6b). Due to the stress cushioning-effect of the glass, the stress was lowered by 62.5%, which means that the zero-point output was lowered by 62.5%. High zero-point output will impose restrictions on low power applications. So, the sensor with bonded glass was not easily influenced by packaging stress and had better performance.

E. FEM Analysis for the Effect of Passivation Films

Pressure sensor chips need to be covered by passivation films. The films were used to stop water vapor and impurities to pollute sensor chips. They also served as inter metal layer dielectric to ensure the electrical properties of Wheatstone bridge. However, bad effects were also caused [9]. Passivation films were fabricated by LPCVD (low pressure chemical vapor deposition). Stress was supposed to 0 when the films were deposited at 720 °C. But when the temperature was decreased to 25 °C, stress will be induced due to the difference of coefficients of thermal expansion of silicon substrate and passivation films.

Under the thermal mismatch stress, the sensing diaphragm will be deformed. Consequently, on the one hand, zero-point

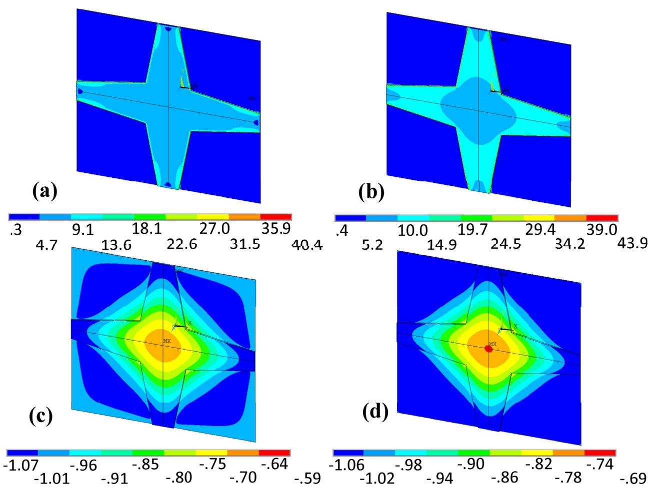

Fig. 7. Simulation for the effect of passivation films on the sensing diaphragm: Von Mises stress distribution for the shuriken structured diaphragm (shuriken deposited by 250 nm SiO_2 (a) and 350 nm SiO_2/110 nm Si_3N_4 (b)); Z-Component of displacement distribution for the shuriken structured diaphragm (shuriken deposited by 250 nm SiO_2 (c) and 350 nm SiO_2 /110 nm Si_3N_4 (d)).

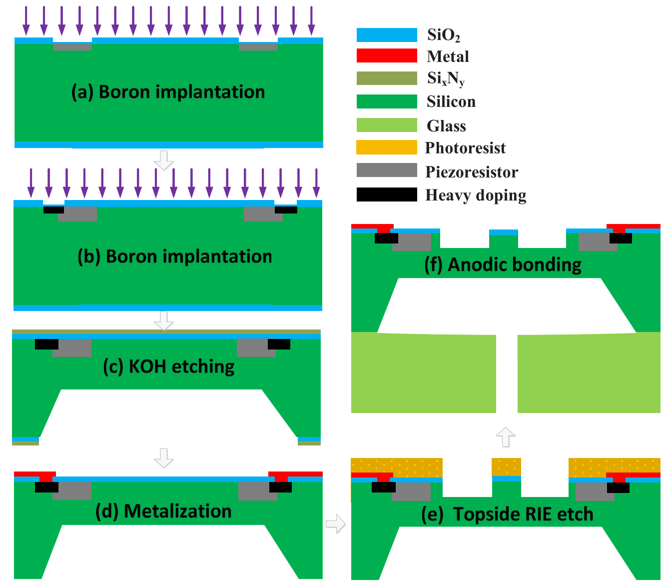

Fig. 8. The fabrication process flow.

TABLE I
EXPERIMENT DESIGNS

	SiO_2	SiO_2/Si_3N_4	Bonded glass
Experiment 1	√	×	×
Experiment 2	×	√	×
Experiment 3	√	×	√

voltage output will drift. This will also impose restrictions on low power applications. On the other hand, the axial stress of the sensing diaphragm will change the membrane stiffness characteristics so that the sensitivity and linearity of the sensor will be affected. This will make signal processing more complicated.

In this simulation, the elastic moduli (EX) and major Poisson's ratios (PRXY) for silicon are 169 GPa and 0.28, respectively. The instantaneous coefficients of thermal expansion (CTEX) of silicon are from the research of C. A. Swenson [18]. In general, the EX, PRXY and CTEX of SiO_2 are 71.7 GPa, 0.17 and 0.55e-6, respectively. And the EX, PRXY and CTEX of Si_3N_4 are 310 GPa, 0.27 and 3.3e-6, respectively. The simulated results are from FEM analysis.

The Von Mises stress distributions for the shuriken-structured diaphragm (shuriken deposited by 250 nm SiO_2 (Figure 7a) and 350 nm SiO_2/110 nm Si_3N_4 (Figure 7b)) were displayed. Our designed piezoresistive area was in the low thermal stress region, and this will weaken the effect of thermal stress on the sensor performance. Compared with SiO_2, for the sensing films deposited by SiO_2/Si_3N_4, the low stress regions shrinked and correspondingly the high stress region expanded. So, the stress of piezoresistive area was increased and this was not wanted for good sensor performance. Based on piezoresistance effect, the zero-point output voltage for the sensor passivated by SiO_2/Si_3N_4 was -43.0961 mV, which was much less than the zero-point output voltage -22.4194 mV of the sensor passivated by SiO_2. Si_3N_4 films had worse influence on sensor performance.

The deformation of the sensing diaphragm (shuriken deposited by SiO_2 and SiO_2/Si_3N_4) was shown in Figure 7c and 7d, respectively. The similar deformation states were shared. For the whole membrane, the deformation appeared as upward bending type. The deflection of the membrane passivated by SiO_2/Si_3N_4 was a little bit (about 100 nm) less than the membrane passivated by SiO_2. But the average piezoresistor stress passivated by SiO_2/Si_3N_4 film was about the double of that passivated by SiO_2 film. In spite of the tiny deformation change, the large stress change of piezoresistive area should be paid attention to.

III. FABRICATION

The fabrication process flow was shown in Figure 8: (a) SiO_2 film on N (1 0 0) crystal silicon was formed by thermal oxidation process. Some of the SiO_2 film was subsequently thinned to 400-800 μm by RIE (reactive ion etch) to inhibit the channeling effect of the ion implantation process. Piezoresistive area was lightly doped. The silicon piezoresistor dose was 8.5×10^{13} cm^{-2}. The implantation energy was 100 KeV; (b) The heavily doped region was later made to achieve effective ohmic contacts. The boron dose was 5×10^{15} cm^{-2}. The implantation energy was 100 KeV; (c) $SiO_2$and Si_xN_y were deposited sequentially by LPCVD. On the back of the wafer, KOH etching windows were formed first by RIE to remove the Si_xN_y followed by buffer HF erosion to remove SiO_2. The square diaphragm was then fabricated by KOH anisotropic etching; (d) Using lift-off technique, metallization was completed; (e) The SSD was later developed by RIE in the front of the square diaphragm by thinning some part of the diaphragm; (f) Finally, the silicon wafer was bonded with perforated glass by anodic bonding process.

To investigate stress cushioning-effect of the bonded glass and effect of passivation films on sensor performance, a series of comparative experiments were designed shown in Table 1.

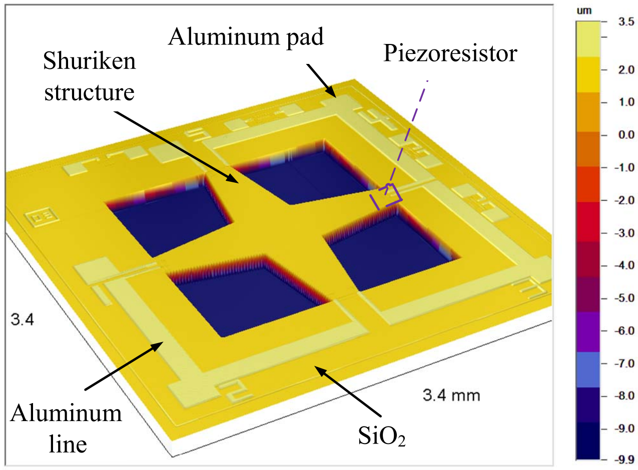

Fig. 9. The fabricated sensor obtained by Bruker non-contact optical surface profiler.

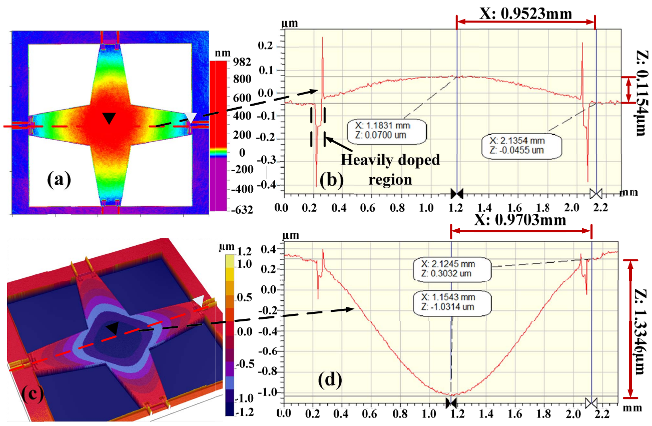

Fig. 10. The deformation of SSD caused by passivation films (tested by Bruker 3D microscope): (a) (b) Shuriken covered by 250 nm SiO_2 (c) (d) Shuriken covered by 350 nm SiO_2/ 110 nm Si_xN_y.

IV. Results

A. The Fabricated Sensor Chip

The fabricated sensor was shown in Figure 9. Different colors represented different altitude. Detailed material and structure information can also be easily got shown in Figure 13. The fabricated SSD sensor had few visual defects and pleasing structural integrity.

B. Effect of Passivation Films

The stress state of the SSD was closely relevant to passivation films (Figure 10). Si_3N_4 films had worse effect on SSD deformation. With shuriken covered by a SiO_2 film, the SSD was bended upward just about 0.1 μm. Nevertheless, with shuriken covered with SiO_2 / Si_xN_y, the SSD was deformed downward approximately 1.3 μm. The SSD sensor covered with SiO_2/Si_xN_y had a slightly smaller sensitivity and a significantly lower linearity in comparison with that covered with SiO_2 shown in Table 2.

Figure 10 also showed that the diaphragm deformation was quite different from our simulation results (Figure 7).

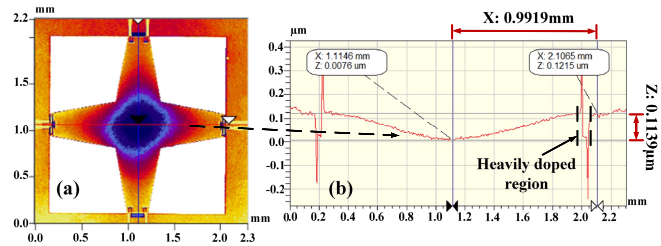

Fig. 11. The deformation of SSD bonded with glass substrate caused by passivation film (250 nm SiO_2).

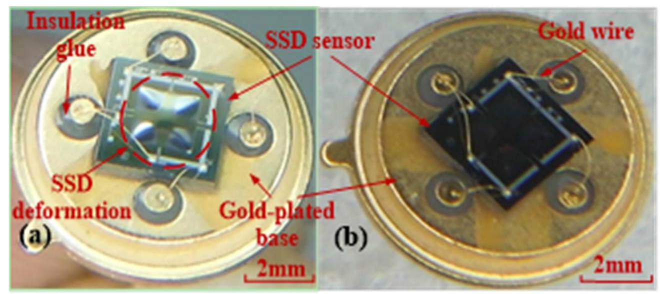

Fig. 12. The deformation of SSD caused by packaging glue between the SSD sensor and gold-plated base: (a) Without and (b) With bonded glass.

Our simulated results showed that the deformation should appear as upward bending type. However, the testing results showed that the deformation appeared as downward bending in Figure 10c and 10d. The most possible reason may be that our fabricated Si_3N_4 were different from our supposed material due to the fabrication environment. Its CTEX were much more than our supposed values.

Figure 11 showed the downward deformation for the SSD sensor with bonded glass. The deflection was about 114 nm. The fabricated glass substrate turned the upward bending (Figure 10a and 10b) to downward state due to the bonding thermal mismatch stress.

C. Influence of Assembly Stress

The SSD sensor was packaged as shown in Figure 12. The sensor was glued to the gold-plated base. Through gold wire bonding, the pads of the sensor were connected with the outer electrodes on the base. The outer electrodes were disconnected electrically by isolation glue.

The performance of the SSD sensor was closely related to the stress state of the SSD. The SSD without bonded glass (Figure 12a) was deformed seriously by packaging glue but only slightly with bonded glass (Figure 12b). For the deformed sensor, zero offset voltage output was higher and device output varied over time which was similar to the creep phenomenon. In terms of the sensor with bonded glass, because of the favorable stress cushioning-effect of the glass, the SSD cannot be easily influenced resulting in better and more stable device performance.

Figure 13 showed the initial upward deformation of the SSD diaphragm after packaging. The deformation cannot be seen directly for Figure 12b. But in Figure 16, the deformation was

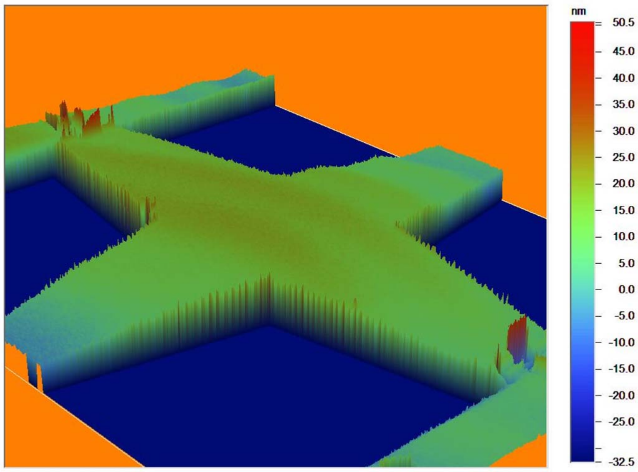

Fig. 13. The initial upward deformation of the SSD diaphragm after packaging.

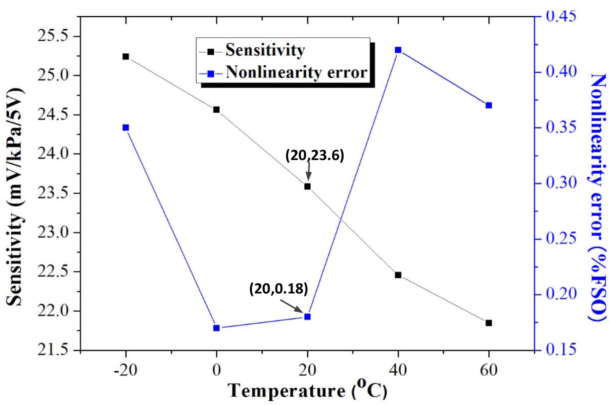

Fig. 14. Sensitivity and nonlinearity error measurement under the condition of temperature varying from −20 °C to 60 °C.

reflected and the maximum deflection was about 83 nm. Due to the assembly stress, the downward bending (Figure 11) was changed into upward state.

D. Device Performance

Test results of the SSD sensor were shown in Figure 14. The sensor had a high sensitivity of 23.6 mV/kPa/5V and low nonlinearity error of 0.18 %FSO at 20 °C. When temperature increased from −20 °C to 60 °C, silicon piezoresistive coefficient decreased so that the sensitivity droped, but still more than 21.5 mV/kPa/5V which can be seen from the black curve in Figure 14. Using linear function to fit the black curve, temperature coefficient of sensitivity was −0.0445 mv/kPa/5V/°C. As for nonlinearity error, it floated up and down with temperature changing (blue curve in Figure 14), but was still less than 0.45 %FSO for which the possible reason may be that the stress state of the SSD had complex relation with temperature. In short, due to the excellent properties of the SSD, the pressure sensor showed a high sensitivity and linearity simultaneously.

Table 2 showed comparative experiments testing results for pressure sensor performance. For experiment 3, the sensitivity

TABLE II

COMPARATIVE EXPERIMENT TESTING RESULTS FOR PRESSURE SENSOR PERFORMANCE

	Exp. 1	Exp. 2	Exp. 3
Sensitivity (mV/kPa/V)	4.12	4.11	4.72
Nonlinearity (FSO%)	0.14	3.33	0.18
Zero off-set (mV)	-7.89	94.20	-5.78

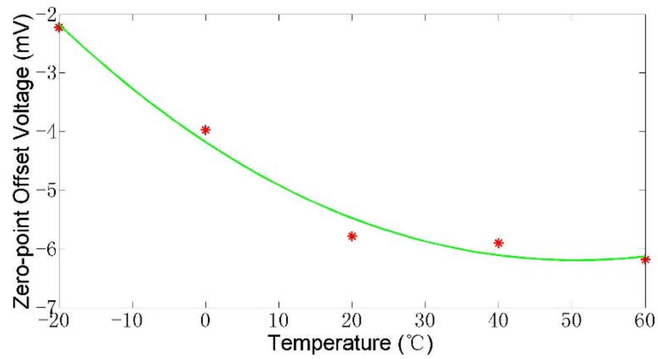

Fig. 15. Zero-point Offset Voltage measurement under the condition of temperature varying from −20 °C to 60 °C.

was the highest, the linearity was medium, and the absolute value of the Zero off-set was the best. For experiment 1, the sensitivity was medium, the linearity was the best, and the Zero off-set was medium. For experiment 2, the sensitivity was the lowest, the linearity was the poorest, and the zero off-set was the worst.

The zero-point offset voltage measurement for experiment 3 under the condition of temperature varying from −20 °C to 60 °C were shown in Figure 15. The negative offset voltage was consistent with the initial upward deformation of the SSD. When temperature increased from −20 °C to 60 °C, the unwanted offset of the sensor decreased from −2.2 to −6.2 mV. The green fitting cure was a cubic polynomial spline. The offset changed quickly at the beginning. After 20 °C, it decreased little with temperature. In general, the offset and its temperature coefficient were low and can be easily compensated by circuits.

Table 3 showed the performance comparison with previously reported typical structures. The sensors shared similar silicon film thickness. High sensitivity means high output voltage. High linearity represents high resolution. Small diaphragm area facilitates low cost and high profits. So high sensitivity, high linearity and small diaphragm area are preferred. Our proposed sensor had the highest sensitivity, a medium nonlinearity and the smallest area. A new performance index P was proposed shown in Equation 7. For our sensor, P was the highest. Compared with our previous work [11], the sensitivity was increased by 28.3%, while the nonlinearity was reduced by 50%.

$$P = \frac{Sensitivity}{(Nonlinearityerror) \times (Diaphragmarea)} \tag{7}$$

TABLE III
PERFORMANCE COMPARISON WITH PREVIOUSLY REPORTED TYPICAL STRUCTURES

Diaphragm type	Sensitivity (mV/kPa/V)	Nonlinearity error (%FSO)	Diaphragm area (mm×mm)	P	Si film thickness (μm)
Shuriken-structured	4.72	0.18	1.9×1.9	7.26	19
Peninsula-structured[10]	3.68	0.36	1.9×1.9	2.83	19
Beam-membrane [11]	1.55	0.09	3×3	1.91	20
Central bossed [12]	3.5	-0.11	3.5×3.5	2.60	20

V. CONCLUSION

In this work, a SSD is introduced for the first time to simultaneously increase the sensitivity and linearity of the piezoresistive pressure sensor. Simulation results indicated that the SSD sensor had a high sensitivity of 4.67 mV/kPa/V and a low nonlinearity of less than 0.1%. Test results reflected that the sensor had a high sensitivity of 4.72 mV/kPa/V and low nonlinearity error of 0.18% FSO at 20 °C. Compared with previously reported typical structures, the SSD structure possessed unique advantages, particularly suitable for the monitoring of IOP and ICP.

The influences of assembly stress and passivation films on the device performance were also studied here. Because of assembly stress, for the SSD sensor, zero offset voltage output was higher and device output may vary over time. SiO_2 / Si_xN_y passivation films brought higher stress onto the SSD and increased the stiffness of the sensing diaphragm, consequently the sensor had worse sensitivity and linearity.

VI. ACKNOWLEDGEMENTS

The authors would like to thank the staff of National Key Laboratory of Science and Technology on Micro/Nano Fabrication for cooperation and help in the fabrications.

REFERENCES

[1] T. Guan *et al.*, "A novel 0–3 kPa piezoresistive pressure sensor based on a Shuriken-structured diaphragm," in *Proc. IEEE 29th Int. Conf. Micro Electro Mech. Syst. (MEMS)*, Jan. 2016, pp. 816–819.
[2] M. B. Sultan and S. L. Mansberger, P. P. Lee, "Understanding the importance of IOP variables in glaucoma: A systematic review," *Surv. Ophthalmol.*, vol. 54, no. 6, pp. 643–662, 2009.
[3] D. K. Gupta, H. Kumar, and A. K. Mahapatra, "Role of invasive ICP monitoring in patients with traumatic brain injury: An experience of 98 cases," *Indian J. Neurotrauma*, vol. 3, no. 1, pp. 31–36, 2006.
[4] S. Marco, J. Samitier, O. Ruiz, J. R. Morante, and J. Esteve, "High-performance piezoresistive pressure sensors for biomedical applications using very thin structured membranes," *Meas. Sci. Technol.*, vol. 7, no. 9, pp. 1195–1203, 1996.
[5] W. J. Fleming, "Overview of automotive sensors," *IEEE Sensors J.*, vol. 1, no. 4, pp. 296–308, Dec. 2001.
[6] C. Debes, A. Merentitis, S. Sukhanov, M. Niessen, N. Frangiadakis, and A. Bauer, "Monitoring activities of daily living in smart homes: Understanding human behavior," *IEEE Signal Process. Mag.*, vol. 33, no. 2, pp. 81–94, Feb. 2016.
[7] W. P. Eaton and J. H. Smith, "Micromachined pressure sensors: Review and recent developments," *Smart Mater. Struct.*, vol. 6, no. 5, pp. 530–539, 1997.
[8] L. Lin, H.-C. Chu, and Y.-W. Lu, "A simulation program for the sensitivity and linearity of piezoresistive pressure sensors," *J. Microelectromech. Syst.*, vol. 8, no. 4, pp. 514–522, Dec. 1999.
[9] J. Chiou and S. Chen, "Pressure nonlinearity of micromachined piezoresistive pressure sensors with thin diaphragms under high residual stresses," *Sens. Actuators A, Phys.*, vol. 147, no. 1, pp. 332–339, 2008.
[10] K. Matsuda, K. Suzuki, K. Yamamura, and Y. Kanda, "Nonlinear piezoresistance effects in silicon," *J. Appl. Phys.*, vol. 73, no. 4, pp. 1838–1847, 1993.
[11] X. Huang and D. Zhang, "A high sensitivity and high linearity pressure sensor based on a peninsula-structured diaphragm for low-pressure ranges," *Sens. Actuators A, Phys.*, vol. 216, pp. 176–189, Sep. 2014.
[12] B. Tian, Y. Zhao, Z. Jiang, and B. Hu, "The design and analysis of beam-membrane structure sensors for micro-pressure measurement," *Rev. Sci. Instrum.*, vol. 83, no. 4, p. 045003, 2012.
[13] H. Sandmaier and K. Kuhl, "A square-diaphragm piezoresistive pressure sensor with a rectangular central boss for low-pressure ranges," *IEEE Trans. Electron Devices*, vol. 40, no. 10, pp. 1754–1759, Oct. 1993.
[14] C. S. Smith, "Piezoresistance effect in germanium and silicon," *Phys. Rev.*, vol. 94, pp. 42–49, Apr. 1954.
[15] K. Hoffmann, "Applying the wheatstone bridge circuit," Hottinger Baldwin Messtechnik, Darmstadt, Germany, Tech. Rep. HBM S1569-1.1 en., 1974.
[16] Y. WC and B. RG, *Roark's Formulas for Stress and Strain*, 7th ed. New York, NY, USA: McGraw-Hill, 2002.
[17] L. D. Landau and E. M. Lifshitz, *Theory of Elasticity*, vol. 7. Course of Theoretical Physics, Butterworth-Heinemann, Oxford, U.K.: 1986. Landau, Lev
[18] C. A. Swenson, "Recommended values for the thermal expansivity of silicon from 0 to 1000 K," *J. Phys. Chem. Reference Data*, vol. 12, no. 2, pp. 179–182, 1983.

Taotao Guan received the B.S. degree in microelectronics from the University of Electronics Science and Technology of China, Chengdu, China, in 2014.

He is currently pursuing the Ph.D. degree in micro-electro-mechanical system (MEMS) with the National Key Laboratory of Science and Technology on Micro/Nano Fabrication, Institute of Microelectronics, Peking University, Beijing, China. His current research interests include pressure sensor, piezoressitive effect, HNA etching, MEMS reliability, and micro/nano-mechanical test on chip.

Fang Yang received the M.S. degree in 2004. She was with the National Key Laboratory of Science and Technology on Micro/Nano Fabrication, for 12 years, Beijing, China.

She has finished the fabrication of dozens of MEMS devices, such as gyroscope, accelerometer, pressure sensor, and flow meter. She is experienced in MEMS micro/nano-fabrication. She has co-authored 31 papers and applied for 37 patents for invention (two international patents and 20 patents authorized). Her research mainly focuses on MEMS fabrication technology and its reliability.

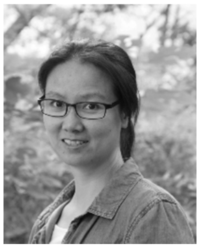

Wei Wang received the B.Eng. degree from China Agricultural University, Beijing, China, in 1994. She was with the National Key Laboratory of Science and Technology on Micro/Nano Fabrication, for 12 years, Beijing, China.

She became a Senior Engineer in 2004. She has undertaken many research projects, such as PVD film study and nanometer device fabrication. She applied for 26 patents for invention (six authorized). Her research interests include PVD film fabrication and MEMS fabrication process optimization and management.

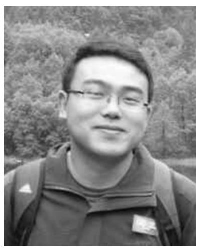

Xian Huang was born in 1988. He is currently with the Shenzhen Graduate School, Peking University, Shenzhen, China. He is currently pursuing the Ph.D. degree from the Institute of Microelectronics, Peking University, Beijing, China. His main research interests include micro/nano fabrication technology and MEMS piezoresistive devices.

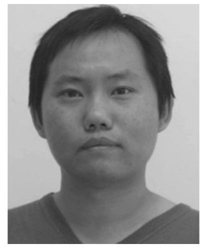

Boyan Jiang received the M.Eng. degree in electronics and communications engineering from Peking University, Beijing, China, in 2009.

He is currently with the National Key Laboratory of Science and Technology on Micro/Nano Fabrication, Beijing, China. His research mainly focuses on MEMS fabrication process, such as lithography, bonding and wet etching. He is experienced in the fabrication and test of piezoresistive pressure sensor, MEMS gas sensor, gyroscope, and accelerometer.

Dacheng Zhang received the Ph.D. degree from the Institute of Microelectronics, Peking University, Beijing, China, in 2004. His research interests include silicon-based MEMS fabrication technology, microstructure process-related parameter extraction, MEMS design, and MEMS reliability.

Since 1996, he has undertaken over ten state-level scientific research projects, such as the National High-tech Research and Development Program of China (863 Program), the National Program on Key Basic Research Project of China (973 Program), the National Natural Science Foundation of China (NSFC), and the National Science and Technology Major Project of the Ministry of Science and Technology of China. He has authored or co-authored over 30 papers (over 20 SCI papers), and applied for over 40 patents for invention (over 30 authorized). He came up with the China‘s first MEMS field international standard proposal named after Silicon based MEMS fabrication technology-Measurement method of pull-press and shearing strength of micro bonding area.

Dr. Zhang, was a recipient of many outstanding honors, such as the First Class Prize of Beijing Science and Technology Progress Award in 2003, the Second Class Prize of the State Award for Inventions in 2006, and the Second Class Prize of the Ministry of Education Science and Technology Progress Award.